Journal of Physics D: Applied Physics

PAPER

Influence of internal stress and layer thickness on the formation of hydrogen induced thin film blisters in Mo/Si multilayers

To cite this article: R A J M van den Bos *et al* 2018 *J. Phys. D: Appl. Phys.* **51** 115302

View the article online for updates and enhancements.

Related content

- Blister formation in Mo/Si multilayered structures induced by hydrogen ions
  R A J M van den Bos, C J Lee, J P H Benschop et al.
- Influence of near-surface blisters on deuterium transport in tungsten
  J. Bauer, T. Schwarz-Selinger, K. Schmid et al.
- Reactive diffusion in multilayer metal/silicon nanostructures
  Evgenii N Zubarev

This content was downloaded from IP address 130.89.46.45 on 23/05/2018 at 10:33

IOP Publishing Journal of Physics D: Applied Physics

J. Phys. D: Appl. Phys. **51** (2018) 115302 (11pp) https://doi.org/10.1088/1361-6463/aaad86

Influence of internal stress and layer thickness on the formation of hydrogen induced thin film blisters in Mo/Si multilayers

R A J M van den Bos[1], J Reinink[1], D V Lopaev[2], C J Lee[1,3], J P H Benschop[1,4] and F Bijkerk[1]

[1] Industrial Focus Group XUV Optics, MESA + Institute for Nanotechnology, University of Twente, Enschede, Netherlands
[2] Skobeltsyn Institute of Nuclear Physics, Moscow State University, Moscow, Russia
[3] Insitute of Engineering, Hogescholen Fontys, Eindhoven, Netherlands
[4] ASML Netherlands B.V., Veldhoven, Netherlands

E-mail: r.a.j.m.vandenbos@utwente.nl

Received 25 November 2017, revised 29 January 2018
Accepted for publication 7 February 2018
Published 22 February 2018

Abstract

A Mo/Si multilayer film may blister under hydrogen exposure. In this paper, we investigate the impact of intrinsic stress on blister formation in multilayers by varying the Si thickness between 3.4–11 nm and changing the hydrogen ion exposure conditions. Increasing the thickness of a-Si is found to introduce a higher average compressive stress in the multilayer film. Measurements of the average film stress before and after hydrogen exposure did not reveal a correlation between stress relaxation and the observation of surface blisters. Comparing the experimentally observed blister size distribution to that predicted by elastic models of blistering due to pressure, and thin film buckling showed that increasing hydrogen pressure under the blister cap is the main cause of the observed blisters. It is also shown that hydrogen diffusion plays an essential role in the blister formation process as sufficient hydrogen is required to pressurize the blister.

Keywords: blister formation, Bragg reflector, multilayer stress, hydrogen

S Supplementary material for this article is available online

(Some figures may appear in colour only in the online journal)

1. Introduction

Material degradation due to exposure to hydrogen is a topic of extensive research [1–5]. Over the years many damaging processes have been identified, of which, hydrogen induced blister formation is one [1, 2]. Blister formation is of relevance for a diverse range of applications, from the development of plasma-facing materials for fusion reactors [6–9], to silicon-on-insulator transfer processes [10, 11]. As a result, a considerable amount of information on hydrogen uptake, diffusion, and blistering in homogeneous materials has been published [1, 2, 12–14]. Most research on blistering has, so far, focused on semiconductors [2, 15], and metals [6, 7, 16].

In this article, we focus on blister formation in heterogeneous Mo/Si multilayer mirrors. These mirrors are created by depositing alternating nanometer thick molybdenum and silicon layers on a substrate, which forms an artificial Bragg crystal that is able to reflect light at a specific wavelength. Mo/Si multilayer mirrors can be found in the optical systems of, for example, space telescopes, synchrotrons, and extreme ultraviolet lithography [17–19]. During the optics' lifetime, mirrors may be exposed to hydrogen to remove contaminants

 © 2018 IOP Publishing Ltd Printed in the UK

from the surface and maintain optimal reflectivity. However, under some conditions, this has led to the formation of blisters, as can be seen in the TEM images of figure 1.

The basic qualitative picture of hydrogen induced blister formation is now well understood and, mainly, two mechanism for blister formation can be found in literature. The first mechanism is related to material deformation under high hydrogen pressure building up in nanometer-scale cavities near the surface [2]. Alternatively, circular blister growth can be caused by a buckling instability of a compressively stressed thin film [20–22].

Together with the above blister mechanisms, several elastic models have been developed that relate the final observed blister dimensions to the intrinsic stress and/or pressure required to be able to deflect the blister cap [20, 21, 23–27]. Although these models give an estimate of the internal hydrogen pressure and/or critical compressive stress, they do not explain the microscopic processes involved in the initial stage of the blister formation, where hydrogen diffusion leads to cracking and trapping of hydrogen at a certain depth.

As these microscopic processes depend on many parameters in both exposure conditions and material properties, it is difficult to predict if and when blistering will occur in a given material. For example, it has been shown that nanometer sized $Si/Si_{1-x}Ge_x/Si$ layered structures have a completely different susceptibility to blistering, compared to that for a homogeneous Si bulk material [28, 29].

To better understand the blistering behavior of Mo/Si multilayers, it is, therefore, required to understand both hydrogen diffusion through the multilayer, and the relative importance of stress and hydrogen pressure for blister formation. In previous work on blistering in Mo/Si multilayers, only the dependence on exposure conditions e.g. substrate temperature, flux and ion energy has been investigated [30–32]. In this work, the structure of the multilayer is changed by varying the silicon thickness. This changes both the thickness of the blister cap, and the compressive stress in the blister cap. In this way, the relative significance of elastic buckling [20, 21], and pressure-driven elastic deformations [27] is evaluated. To minimize the structural changes to the multilayer, the polycrystalline Mo layer thickness is kept constant for all multilayers.

First, the internal stress development in a Mo/Si multilayer is discussed in detail in section 3.1. After that, the changes in internal stress due to exposure to hydrogen are discussed in section 3.2. In the last section 4, the experimentally observed blisters in the multilayer are discussed. First, the location of crack formation in the multilayer is explained in section 4.1. Then, the observed blister sizes are compared to that predicted from elastic models for blister formation caused by either buckling or hydrogen pressure,in section 4.2 [20, 21, 27, 33]. Finally, in section 4.3, the required local hydrogen ion dose, calculated from the pressurized blister model, is compared with the amount of hydrogen that penetrates to the crack region. The dose is estimated from exposure measurements, combined with SRIM calculations and a 1D diffusion model.

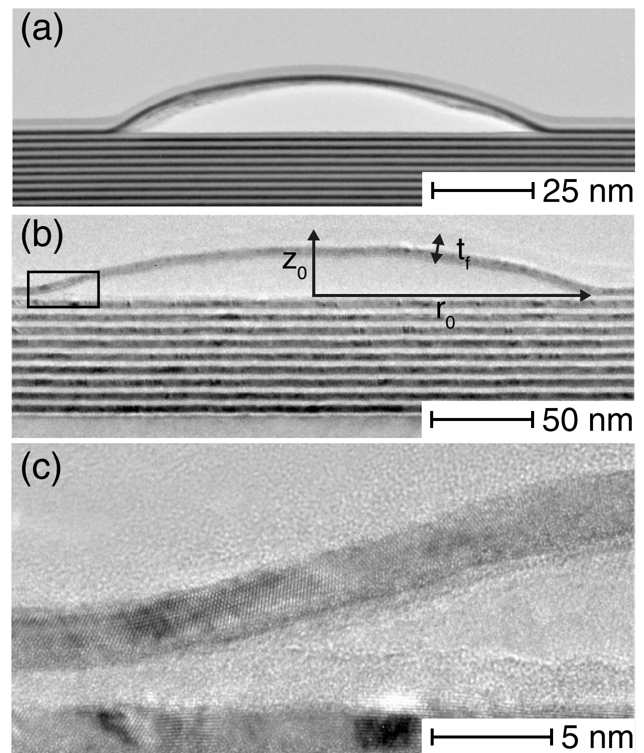

Figure 1. TEM images of nanometre sized blisters, formed near the surface of a Mo/Si multilayer mirror after exposure to 100 eV hydrogen ions. Complete blister in a 8.2 nm (a) and 6.4 nm (b) period Mo/Si multilayer. (c) Magnified image of one of the blister edges as indicated by the rectangle in (b). Arrows indicate the blister dimensions as used in the text: maximum deflection z_0, blister radius r_0, and blister cap thickness t_f.

2. Materials and methods

2.1. Mo/Si multilayer sample preparation

Nanometer thick silicon and molybdenum layers were deposited on top of a 25 × 25 mm^2 polished Si(1 0 0) substrates (thickness: $157 \pm 2\,\mu$m) using magnetron sputtering. Between the first deposited a-Si layer and the Si(1 0 0) substrate a thin layer of native oxide was present. Each sample had a total of 10 Mo/Si bilayers deposited. This is sufficient to avoid any influence from the substrate on hydrogen penetration and stress development in the Mo/Si bilayer. To vary the average intrinsic stress in the bilayer, the period of the multilayer was changed by increasing the silicon layer thickness. In total 4 different sample periods, varying from 6.4 nm to 14.0 nm, were deposited, as shown in figure 2. The thickness of the Mo layer including the interface layers was kept constant at 4.6 nm.

From literature it is known that Mo-on-Si and Si-on-Mo interfaces are formed with quite different thicknesses and stoichiometry [34–36]. The Mo-on-Si interface has a thickness of 1.8 nm with $MoSi_2$ stoichiometry and the Si-on-Mo interface has a thickness of 0.4 nm with a Mo_5Si_3 stoichiometry as measured by [34]. These interface thicknesses are depicted to scale in figure 2 next to the HRTEM images. The thickness of the Mo including both interfaces is comparable to the distances between changes in contrast as seen in the HRTEM

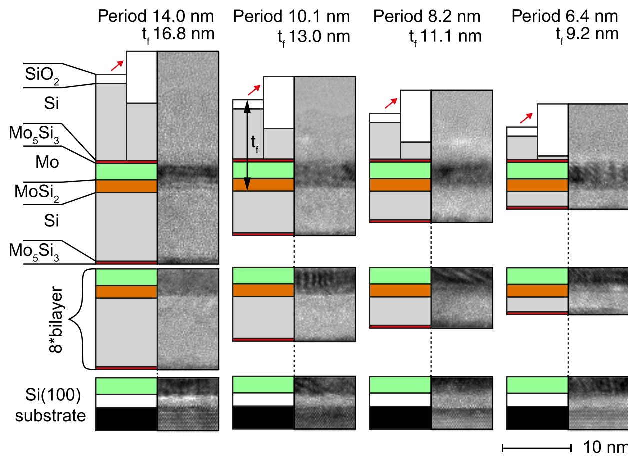

Figure 2. Schematic picture and corresponding HRTEM image of the Mo/Si multilayer samples with four different periods. The period is varied by increasing the a-Si thickness. The Mo-on-Si and Si-on-Mo interfaces are indicated by different colors. After hydrogen exposure the silicon oxide thickness on top of the multilayer increases as indicated by the red arrows (left: initial oxidation, right: oxidation after hydrogen exposure).

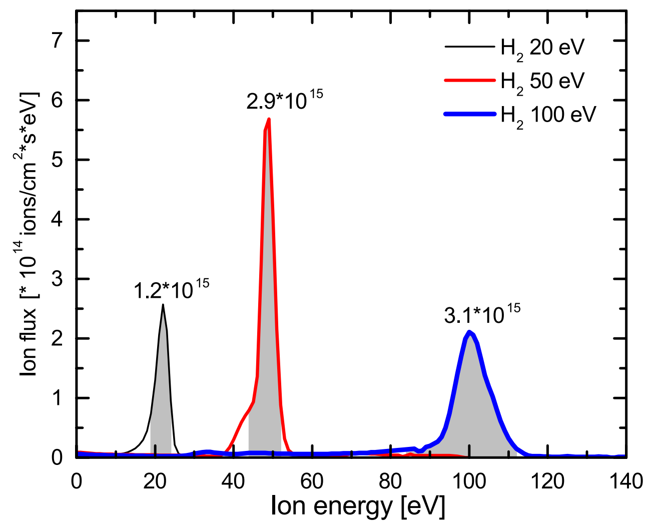

Figure 3. Ion energy density function (IEDF) of the hydrogen plasma for three different ion energies. Total ion flux, ϕ, in ions cm^{-2} s is indicated above the peaks. 80% of ion production is within the indicated gray area.

images. The bilayer period of the samples was confirmed using grazing incidence x-ray reflectivity (see supplemental material for the XRR measurement data and model fit (stacks.iop.org/JPhysD/51/115302/mmedia)). This technique is commonly used to determine layer thicknesses in Mo/Si multilayers with an accuracy of $\approx$0.1 nm [37, 38]. X-ray reflectivity measurements also show that the terminating a-Si layer is oxidized to a depth of $\approx$1.3 nm.

2.2. Hydrogen exposure conditions

Multilayer samples are exposed to hydrogen ions by placing the samples on top of one of the electrodes of a dual-frequency capacitively coupled plasma (DF-CCP) system (see supplemental material for a schematic overview and detailed description of the setup). The use of an rf plasma for hydrogen exposures avoids possible surface charging of the sample surface, which occurs in the case of low conductivity materials, such as the terminating oxide of the multilayer samples.

The multilayer samples were exposed to three different ion energies with main ion energy peaks at $\approx$20, 50, and 100 eV. Before and after the samples were exposed, the ion flux and energy distribution at the electrode surface was measured using self-biasing and a retarding field energy analyzer (RFEA), as explained in more detail by [39]. The measured ion energy distribution function (IEDF) and total ion flux at the electrode surface for each exposure condition are shown in figure 3. By controlling the applied electrode voltages and frequencies of the DF-CCP discharge, IEDFs with a single narrow peak (FWHM $\lesssim$ 10 eV) could be generated.

The composition of the ion species was measured with an enhanced quadrupole plasma analyzer (EQP, Hiden analytical). The EQP measures the IEDF for each ion specie independently. By integrating the IEDF signal of the EQP and correcting for the transmittance and detector sensitivity, the number density of a specific ion in the plasma can be determined. For the exposure conditions at 50 and 100 eV, a ratio of H^+/ H_2^+/ H_3^+ of 20/30/40 is found.

To ensure that exposure conditions were directly comparable, four multilayers with different periods were exposed simultaneously. The samples were placed on a water cooled circular electrode (diameter $\approx$122 mm), in order to maintain a sample temperature less than 25 °C during exposure and to exclude any temperature dependence from our measurements. The hydrogen pressure during operation was stable at 200 mTorr (20 eV) and 20 mTorr (50 and 100 eV). The total hydrogen dose to the sample surfaces was varied between 10^{17}–10^{19} ions cm^{-2} resulting, under the given ion fluxes, to exposure times in the range of 40–16 000 s. Some of the hydrogen exposed samples were excluded from analysis due to the failure of the cooling system.

2.3. Stress measurements

The average stress of an isotropic thin film, deposited on a substrate, can be calculated from the curvature of the substrate. The relation between substrate curvature and the force per unit width applied by the thin film to the bent substrate is given by Stoney's equation [40–42]:

$$\sigma t = -\frac{1}{6}\frac{E_s t_s^2}{1-\nu_s}\frac{1}{R} \tag{1}$$

with σ the average film stress (Pa), t the deposited film thickness (m), E_s Young's modulus of the substrate (Pa), ν_s Poisson's ratio of the substrate, t_s the substrate thickness, and R the radius of curvature of the substrate (m). From equation (1), it can be concluded that the average stress in the film can be determined independently of the elastic properties of the deposited film.

The substrate curvature, R, was determined *ex situ* with an optical surface profiler (Zygo, NewView 7200) and *in situ* using a parallel laser beam apparatus similar to the

experimental method used by [43]. The *in situ* measurement was used to measure the stress changes in the multilayer film in real-time during deposition, while the *ex situ* stress measurements were used to measure changes in the total film stress.

For the *ex situ* measurement a 11×11 mm^2 height map of the surface was created with nanometer height resolution using a surface profiler. The curvature of each substrate was measured three times: before multilayer deposition, after multilayer deposition and after hydrogen exposure. Due to sample cutting, each sample has a slightly different curvature, so the initial substrate curvature is used for background subtraction. Together with the measured period of the multilayer film, the average stress of a single bilayer was calculated.

For *in situ* stress measurements, the relative deflection of two parallel laser beams is used to monitor the bending of a substrate cantilever during deposition. One laser beam (the reference beam) is incident close to the fixed end of the cantilever while to other laser beam (deflected beam) is incident near the free end of the cantilever. After reflection from the cantilever, both laser spots are imaged using a single CCD camera. When the curvature of the cantilever changes, i.e. due to the multilayer deposition, the deflection of the laser beam pointed at the free end of the cantilever will strongly change. The relative curvature change is measured by measuring the change in distance between the two laser spots on the CCD camera during deposition (see supplemental material for a more detailed schematic of the setup geometry). To obtain absolute, rather than relative stress changes, the curvature of the cantilever was measured *ex situ* before and after deposition. The *in situ* stress measurement (as described in section 3.1) was performed on a single cantilever substrate, placed at the same distance from the magnetron targets as for the samples prepared for hydrogen exposure.

3. Results

3.1. Stress development in Mo/Si multilayer films by varying the silicon thickness

To understand the internal stress development in the multilayer with increasing a-Si thickness, changes in the force per unit width of the multilayer were monitored during deposition on a cantilever. In figure 4, the stress development in a single Mo–Si bilayer is shown as a function of deposition time. The linear growth rates for Mo and Si were determined by x-ray reflectivity to be 0.175 nm s^{-1} and 0.245 nm s^{-1} respectively (see supplemental material). The final a-Si thickness of a bilayer was varied between 2 and 12 nm with steps of 2 nm. The Mo thickness, including both Mo_ySi_x interfaces, was held constant at ≈3 nm. The traces in figure 4 have been given an offset for visibility. To reduce the measurement noise, each trace is an average over 5 consecutive deposited bilayers. Except for measurement noise, no significant difference in stress development was observed between the 5 bilayers. All bilayers were deposited on top of each other in the sequence indicated by the numbers in figure 4. In total 41 bilayers were deposited on a single cantilever substrate. The first 12 nm thick Mo/Si bilayer, which was deposited directly on top of

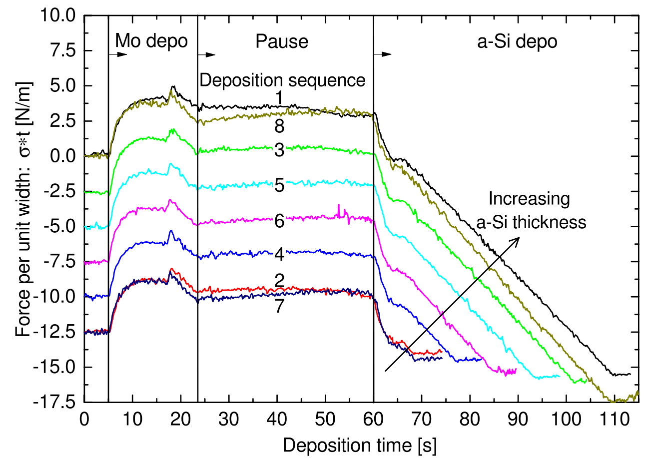

Figure 4. Force per unit width of Mo–Si deposited bilayer films with silicon thicknesses between 2 and 12 nm. An offset (in step sizes of −2.5 N m^{-1}) is added for visibility. The sequence in the deposition is indicated by numbers 1–8.

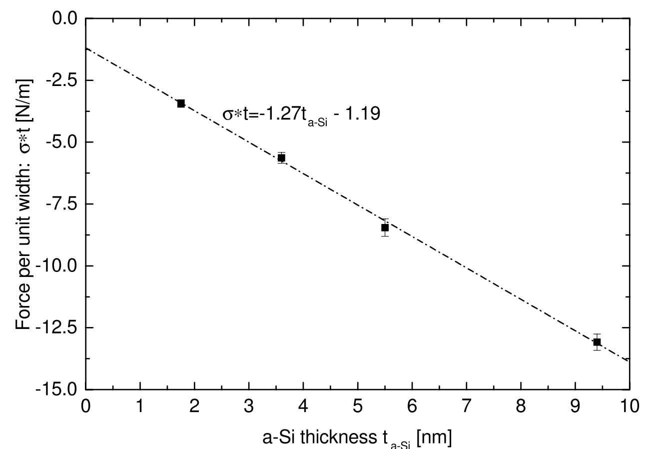

Figure 5. Force per unit width of a bi-layer film with increasing a-Si thickness. The total compressive force of the bi-layer increases with increasing amount of deposited a-Si.

the silicon substrate, was removed from the data as it showed different stress development because of the a-Si/native oxide interface formation.

In the first 10 s of the Mo deposition, a strong tensile curvature change of +4 N m^{-1} is observed. In this early stage, the $MoSi_2$ interface forms, and Si and Mo inter-diffuse [34, 44]. After ≈13 s, the amorphous Mo layer crystallizes to a poly-crystalline molybdenum layer, as can be seen by sudden increase in tensile stress. After crystallization the Mo layer continues to grow under a constant compressive stress of ≈−1.4 GPa, assuming the above 0.175 nm s^{-1} growth rate, and no change in the stress for material at greater depths.

When Si is deposited on top of Mo, the Si intermixes with the Mo to form Mo_5Si_3 during the first 5 s of the Si deposition [34]. After this, the layer grows compressively until Si deposition is stopped. From the slope of the graph, an a-Si layer intrinsic stress of ≈−1.4 GPa is calculated (assuming an a-Si growth rate of 0.245 nm s^{-1}). Similar *in situ* stress measurements by [43] of e-beam deposited Mo/Si multilayers have shown a compressive stress of ≈−1.2 GPa.

Table 1. Relative stress change, $\Delta\sigma/\sigma$, in the Mo/Si multilayer under different hydrogen exposure conditions. Blistered samples are shown in bold. For the 6.4 nm period, four exposures were repeated. The last two columns give the average of the relative stress change and the average of the absolute change in the force per unit width of the multilayer.

		$\Delta\sigma/\sigma$ ($\pm$0.05)				
Period (nm)	Dose (ions cm^{-2})	20 (eV)	50 (eV)	100 (eV)	Average $\Delta\sigma/\sigma$	$\Delta\sigma_f t_f$ (N m^{-1})
6.4	1×10^{17}	−0.10	0.00/−0.10	**− 0.01**	−0.12	4.1 ± 2.0
	1×10^{18}	−0.15	**− 0.12**/ **− 0.10**	**− 0.11**		
	1×10^{19}	−0.19	**− 0.07**/ **− 0.25**	−0.13/**− 0.13**		
8.2	1×10^{17}	−0.07	0.02	−0.07	−0.06	3.5 ± 2.9
	1×10^{18}	−0.05	**0.02**	**− 0.09**		
	1×10^{19}	−0.12	**− 0.09**	**− 0.11**		
10.1	1×10^{17}	−0.01	0.00	−0.01	−0.05	3.9 ± 3.5
	1×10^{18}	−0.07	−0.07	**− 0.06**		
	1×10^{19}	−0.03	**—**	**− 0.12**		
14.0	1×10^{17}	0.00	0.01	−0.05	−0.03	4.5 ± 4.6
	1×10^{18}	0.01	−0.05	−0.03		
	1×10^{19}	−0.07	**− 0.04**	**− 0.09**		

The thinest (2 nm a-Si) and thickest (12 nm a-Si) bilayer series were deposited twice. Once near the start and once near the end of the deposition run. Comparing both graphs for identical a-Si thickness (traces 1 and 8, and traces 2 and 7), it is observed that the slope changes with the total number of deposited bilayers. This effect is due to the different thermal expansion coefficients of the multilayer and the substrate, which generates an additional, thickness-dependent, curvature. As a first order approximation (for $t_f \ll t_{\mathrm{Si}(1\,0\,0)}$), this additional change in curvature with respect to temperature is linear with the total multilayer film thickness. In calculating the a-Si stress value above, this temperature-induced increase in curvature was removed from the data.

The increase in compressive stress in the bi-layer was also measured *ex situ* for the samples prepared for hydrogen exposure (see figure 5). To calculate the force per unit width of a single bilayer, it is assumed that all 10 deposited Mo–Si bilayers are identical. The error shown in the graph is the standard deviation of 9 measured samples. From the slope, an intrinsic stress in the a-Si layer of -1.27 ± 0.03 GPa is determined. This is comparable to the stress value of the *in situ* ($\approx$−1.4 GPa) stress measurement. The average stress in the Mo layer, including both interfaces, was calculated to be -0.26 ± 0.03 GPa from the axis crossing at zero a-Si thickness, assuming a thickness of 4.6 nm. Although the average stress in the Mo layer is low, it can be seen in figure 4 that the highly compressive Mo-on-Si interface nearly cancels the tensile stress in the Si-on-Mo interface, resulting in a small net compressive stress.

3.2. Stress relaxation due to hydrogen exposure

The effect of hydrogen exposure on the average thin film stress was determined by measuring the wafer curvature *ex situ* before and after exposure. The relative stress changes are given in table 1. In calculating the change in stress, we assumed that the substrate and total film thickness are unaffected by hydrogen exposure. The exposures that resulted in a blistered surface are indicated in bold.

The table shows that blisters are formed by either increasing the ion energy or dose. Also, with increasing period thickness, more severe exposure conditions are required before blisters appeared at the surface. This due to the greater depth that hydrogen must penetrate to reach the preferred location for delamination (see sections 4.1 and 4.3). From table 1 it is seen that there is no direct correlation between the appearance of blisters and the relative stress change in the multilayer. Since a blister only changes the stress locally in the top bilayer, and the surface area covered by blisters is typical less than 10%, the stress change due to blistering, averaged over the entire multilayer is quite small. Given the relative measurement uncertainty of 0.05 over the complete 10 bilayer multilayer film, a detectable change in the top layer's stress requires the relaxation of at least half the compressive stress in the top bilayer.

Although the measurement error is too high to make clear statements between the different hydrogen exposure conditions, a trend is still visible in the average stress relaxation. With increasing period, the relative stress change decreases. By multiplying the average relative stress change by the total initial stress in the multilayer, the absolute stress relaxation in the multilayer can be calculated (last column table 1). The typical observed stress change is a $\approx$4 N m^{-1} reduction in compressive stress.

A possible cause of this stress relaxation can be found in the increased oxidation of the a-Si top layer [45, 46]. From the TEM pictures in figure 2 it can be seen that, after hydrogen exposure, the SiO_2 thickness increased to 7.4 nm thickness. This means that an additional $\approx$6.1 nm of SiO_2 has formed after hydrogen exposure which equals an oxidation of $\approx$2.8 nm of a-Si (taking a molar volume expansion of $V_{m,\mathrm{SiO}_2}/V_{m,\mathrm{Si}} \approx 2.17$). Assuming the initial compressively

stressed a-Si is fully relaxed by the oxide growth, and taking the measured compressive stress value of -1.27 N m^{-1} per nm a-Si (see figure 5), the expected stress relaxation due to the additional oxidation is 3.5 N m^{-1}. This is in agreement with the typical measured *ex situ* stress relaxation of 4 N m^{-1} as given in table 1.

From the above discussion, it is clear that the observed stress relaxation is most likely due to oxidation of the a-Si layer, rather than the direct effects of hydrogen exposure.

4. Discussion

4.1. Location of delamination in the Mo/Si multilayer

In figure 1 the HRTEM images show that blisters are formed by the delamination of the first Mo/Si bilayer. As can be seen in the magnified image, figure 1(c), the fracture occurs near the first Mo-on-Si interface in the top of the a-Si layer and not within the $MoSi_2$ interface layer. This is exactly where a strong tensile force change is observed in the *in situ* stress measurement (see figure 4). Based on multiple blisters seen in the HRTEM images of all four multilayer periods, it could be concluded that blisters are preferable formed near the first Mo-on-Si interface similar to the blisters shown in figure 1. Preferred delamination near a highly strained layer has also been observed by [28] in Si/SiGe/Si layered structures.

Another explanation for the location of delamination can be found in the formation of the $MoSi_2$ interface, as investigated in more detail by [44]. When Mo is deposited on Si, clusters of molybdenum silicide are formed on top of the initial silicon surface. To supply the Mo_ySi_x clusters with enough silicon, nearby silicon is transported from its initial position in the silicon surface to the clusters. The removal of silicon to form the interface, leads to nanometer sized cavities in the top of the a-Si layer which can serve as a preferred location for the trapping of hydrogen. Also the formation of cavities might lead to reduced adhesion and mechanical failure between atomic layers as the number density and strength of the atomic bonds is reduced. To better understand the initial stage of blister formation, detailed research on the formation of the interface is required.

4.2. Pressure or buckling induced thin film blister formation

As more hydrogen gets trapped near the $MoSi_2$ interface layer, it can cause the top layer to delaminate. After this initial delamination, a blister can be formed by either buckling of the compressively stressed top layer or by deflection of the top layer under hydrogen pressure. To investigate the role of stress in the final stage of the blister formation process, we studied the statistics of blister radius, r_0, and height, z_0, and compared them to the predictions for elastic models that place a different emphasis on the layer stress. The blister radius, r_0, and height, z_0, was measured by AFM. In figure 6, the measured height and radius of blisters for each multilayer period under different ion dose and ion energy conditions is shown. Note that the ratio of height and radius is approximately

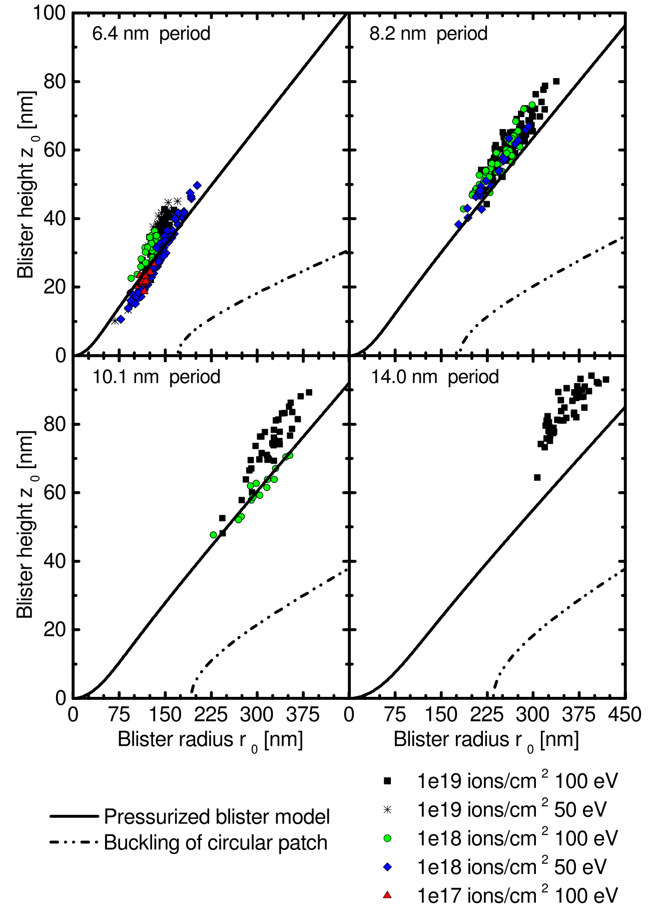

Figure 6. Measured blister height, z_0, versus blister radius, r_0, for different multilayer periods. Model calculations for the pressurized blister model (solid line) and classical buckling of a circular patch (double dot dashed line) are shown [21, 27]. For the pressurized model calculation, a surface energy of $\gamma = 1.87$ J m^{-2} is assumed.

constant, thus, we refer to blister size as height *and* radius. The measurement shows that the blister size increases with multilayer period. In addition, the average blister size for the 6.4 nm period ($\bar{r}_0 = 134$ nm, $\bar{z}_0 = 30$ nm) is comparable with the average blister size found in 7.1 nm Mo/Si period multilayers ($\bar{r}_0 = 100$ nm, $\bar{z}_0 = 19$ nm) as discussed in [32].

Assuming the blisters are caused by increasing hydrogen pressure, the internal hydrogen pressure required to elastically deform the blister cap to the observed shape can be calculated using the pressurized blister model, as described more extensively in [27]. For a given stable blister size, the surface energy and blister pressure are given by:

$$\gamma_{\text{eff}} = 16D\left(\frac{z_0}{r_0}\right)^2\left\{\frac{1}{r_0^2} + \frac{5C}{32t_f^2}\left(\frac{z_0}{r_0}\right)^2\right\} \tag{2a}$$

$$p = 64D\frac{z_0}{r_0}\left\{\frac{1}{r_0^3} + \frac{3C}{16t_f^2}\left(\frac{z_0}{r_0}\right)^2\frac{1}{r_0}\right\}. \tag{2b}$$

Where t_f is the blister cap thickness, D the flexural rigidity (Pa $\cdot$ m^3) and C is a constant that depends on Poisson's ratio only. Assuming ν is 0.22 for a Mo/Si multilayer, $C = 2.51$. γ_{eff} is the effective surface energy in (J m^{-2}), given in equation (3),

Table 2. Layer thickness, Young's modulus (E) and Poisson's ratio (ν) for the top Mo–Si–SiO_2 trilayer [47, 48].

	t_{layer} (nm)	E (GPa)	ν
Mo	4.55	324	0.31
Si	3.3/5.2/7.1/11.0	80	0.22
SiO_2	1.3	71	0.16

where γ is the surface energy. The effective surface energy is the surface energy, reduced by the potential energy stored in the blister cap:

$$\gamma_{\mathrm{eff}} = \gamma - \frac{1-\nu}{2E}\sigma_{\mathrm{int}}^2 t_f. \quad (3)$$

The flexural rigidity of the plate, D, is given by equation (4) with d the distance from the bottom of the plate to the neutral axis, E Young's modulus and ν Poisson's ratio.

$$D = \int_{-d}^{t_f-d} \frac{E(z)}{1-\nu(z)^2} z^2 \mathrm{d}z. \quad (4)$$

To calculate the flexural rigidity of the blister cap, a trilayer structure of Mo, Si, and SiO_2 is considered, with material constants and thicknesses as given in table 2. By calculating the neutral plane, and using equation (4), the flexural rigidity of the blister cap was found to be between, $D = (0.96\text{–}5.88) \times 10^{-14}$ Pa · m^3 for Si layer thicknesses between 3.3 and 11 nm.

Taking the calculated flexural rigidity of the blister cap, and a fixed surface energy of 1.87 J m^{-2} for the Mo-on-Si interface [32], the deflection, z_0, versus the blister radius, r_0, was calculated using equation (2*a*). The result for the various multilayer periods is shown by the solid line in figure 6. It can be seen that the pressurized blister model fits the observed blister measurement data in most cases with a small deviation for the highest dose, ion energy, and thickest silicon layers.

A circular blister can also be formed in the absence of any gas pressure by buckling. The deflection due to buckling can be calculated by solving the nonlinear Föppl–von-Kármán (FvK) plate equations for a clamped circular plate under compressive in-plane stress, as has been extensively discussed elsewhere [20, 21, 33]. To perform the calculation, it is assumed that the circular blister cap has already delaminated from the substrate over a radius r_0, and that $r_0/t_f \ll 1$. When the intrinsic stress exceeds the critical stress, the blister height can be estimated by [21]:

$$z_0 = t_f \sqrt{\frac{1}{c}\left(\frac{\sigma}{\sigma_c} - 1\right)}, \quad (5)$$

where $c = 0.2473(1+\nu) + 0.2231(1-\nu^2)$. This formula becomes asymptotically correct when σ/σ_c approaches 1. The critical stress, σ_c, for a clamped circular patch is given by [20, 33, 49]:

$$\sigma_c = j_1^2 \frac{D}{t_f^3} \frac{1}{(r_0/t_f)^2}. \quad (6)$$

In which $j_1 = 3.8317$ is the first zero crossing of the Bessel function of the first kind. Equation (5) is shown by the double dot dashed line in figure 6 for each period. It is clear that the observed blister height is much higher than predicted by a model purely based on the buckling and that for the 6.4 nm period case blisters are observed below the critical radius of buckling. Therefore, it is expected that, although the blister radius is above the critical blister radius for the 8.2–14.0 nm samples, the main cause of the observed blisters is explained better by hydrogen pressure building up underneath the blister cap.

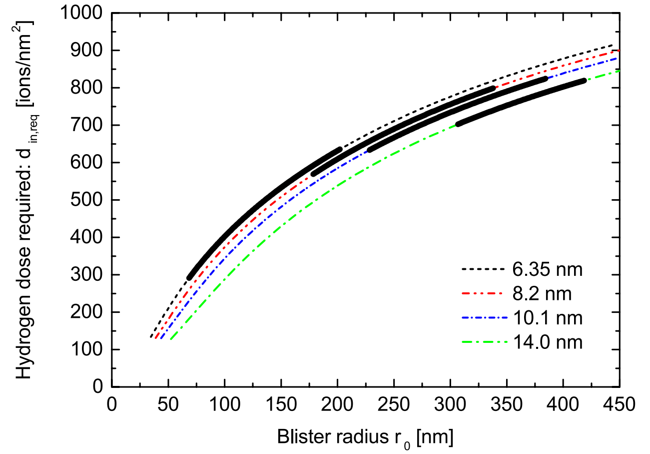

Figure 7. The local hydrogen ion dose required to pressurize a blister of radius r_0 for four different multilayer periods. The range of observed blister radii for each multilayer period are indicated by the thick solid line.

The observed small deviation from the pressurized blister model calculations in figure 6 for the highest dose, ion energy, and thickest silicon layers might be caused by the additional effects of plastic deformation and/or a combined effect of hydrogen pressure and buckling. The measured compressive stress in the multilayer might, therefore, enhance the formation of blisters. In the models explored here, only pure buckling or deflection under hydrogen pressure is taking into account.

4.3. Role of hydrogen diffusion in forming pressurized thin blisters

Assuming that the deflection is initially elastic and neglecting the enhanced deflection of the blister cap above the model calculation as depicted in figure 6, we estimate the hydrogen pressure in the blister using equation (2*b*). The pressure range of the observed blisters is estimated to be between 103 MPa for the largest blisters found on the 14.0 nm period samples to 653 MPa for the smallest blisters found on the 6.4 nm period samples. As the blister aspect ratio z_0/r_0 is nearly constant, it can be seen that the blister pressure decreases along the curve towards larger blister radii.

Based on the blister size and the estimated hydrogen pressure, the amount of trapped hydrogen, N_{H_2}, in a stable blister can also be estimated, following the method discussed in [27]. The calculated local hydrogen ion doses for the four different multilayer periods are shown in figure 7. The range of blister radii experimentally observed are indicated by the thick black line. The graph shows that a local hydrogen ion dose of a few

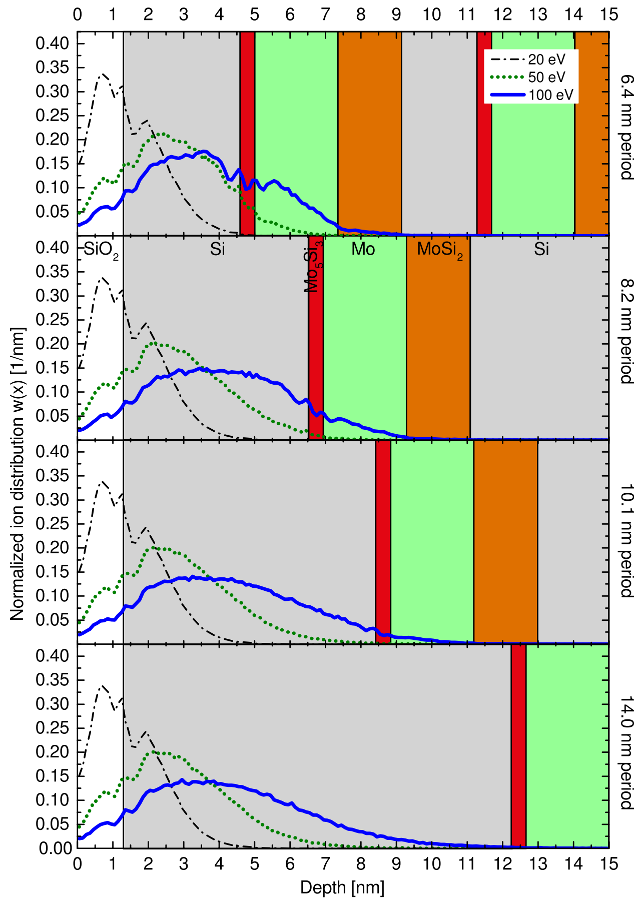

Figure 8. SRIM calculation of hydrogen ion distribution in multilayers with different period and ion energies between 20–100 eV. In these calculations diffusion of hydrogen is neglected and only direct ion penetration due to binary collisions are considered.

hundred ions nm^{-2} is required to form the observed blisters in the multilayer structure. Although this is only a fraction of the total applied ion flux of 10^3–10^5 ions nm^{-2} as measured at the surface (see section 2.2), the dose at the delaminated interface is the more important parameter.

To estimate the amount of hydrogen that can penetrate through the blister cap and enter the blister volume, an SRIM simulation of hydrogen ion penetration was performed for ion energies in the 20–100 eV range [50, 51]. The result of the simulation is shown in figure 8. For the simulation, the trajectories of 2×10^5 hydrogen ions have been simulated. The ion distribution, as given in figure 8, is normalized by the total amount of hydrogen ions. Assuming that the penetration of hydrogen ions is not affected by previous hydrogen ions that have penetrated in the multilayer, the normalized ion distribution is calculated from the probability of finding an ion at a certain depth in the multilayer and the total dose. The amount of directly backscattered ions ranges from 20–30% of the incoming flux, as calculated by the SRIM calculation. The backscattered ions are also taken into account in the normalization of the ion distribution in figure 8.

Ignoring hydrogen diffusion, the local hydrogen ion concentration in the multilayer can be calculated by multiplying the ion distribution (figure 8) with the total measured ion dose of 10^3–10^5 ions nm^{-2}. This results in two main conclusions.

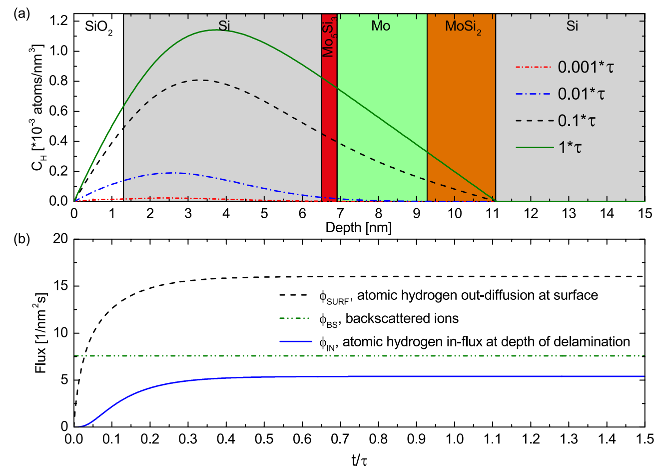

Figure 9. A typical result of the local hydrogen concentration in the multilayer after diffusion for an 8.2 nm period multilayer mirror exposed to 50 eV ions (a). The calculated fluxes to the surface and delamination depth as a function of time are given in (b). The time is normalized to the typical timescale of diffusion $\tau = t_f^2/D_{H_2,\mathrm{eff}} = 4.11$ ms.

Firstly, the amount of hydrogen that accumulates at the delaminated interface is too low to pressurize the blister. And, secondly, the SRIM calculation leads to unrealistically high peak hydrogen ion concentrations in the multilayer (a few hundred to a few thousand ions nm^{-3}). Actual measurements of hydrogen concentrations in hydrogen exposed Mo/Si multilayers have shown typical hydrogen concentration of 10–20 at.% in a-Si [31, 52]. Taking a density of 50 atoms nm^{-3} for c-Si, this means that only a maximum of 5–10 hydrogen atoms nm^{-3} can be stored in the a-Si matrix. Therefore, hydrogen diffusion has to be taken into account.

Since hydrogen exposure is uniform over a lateral length scale of millimeters, while the relevant diffusion lengths are less than a micrometer, we model hydrogen diffusion by numerically solving a time-dependent 1D-diffusion equation:

$$\frac{\partial C_H}{\partial t} = D_{H_2,\mathrm{eff}} \frac{\partial^2 C_H}{\partial x^2} + \phi w(x), \tag{7}$$

in which C_H is the atomic hydrogen concentration in ions nm^{-3}, $D_{H_2,\mathrm{eff}}$ the effective diffusion constant of the blister cap in nm^2 s^{-1}, x the depth in the multilayer in nm, ϕ the ion flux at the surface in ions nm^{-2} s and $w(x)$ the normalized ion distribution resulted from the SRIM calculation, as shown in figure 8. The concentration of atomic hydrogen at the surface and the delamination depth is fixed at 0. We assume that hydrogen ions neutralize and that the concentration of atomic hydrogen outside the multilayer is orders of magnitude less than the concentration within the multilayer. At the delamination region, we assume that hydrogen atoms recombine to form molecular hydrogen, making the atomic hydrogen concentration at the delamination depth negligible. A typical result for the 8.2 nm period multilayer exposed with 50 eV ions is shown in figure 9.

For the effective diffusion constant, the literature value for c-Si is taken: $D_{H_2,\mathrm{eff}} = 2.98 \times 10^{-14}$ m^2 s^{-1} [53]. In figure 9(a), the evolution of the hydrogen concentration profile in the multilayer is shown. Initially, the hydrogen concentration increases

Table 3. Comparison of applied hydrogen ions dose to the blister volume, $d_{\text{in, appl}}$, and required hydrogen ions dose, $d_{\text{in, req}}$, for all exposure conditions. The $d_{\text{in, appl}}$ is calculated from the SRIM depth profile, combined with a 1D-diffusion model. $d_{\text{in, req}}$ follows from the pressurized blister model. For the cases indicated with '—' the sample cooling failed during exposure and these samples were excluded from the analysis.

		20 eV		50 eV		100 eV	
Period (nm)	Dose (ions cm^{-2})	$d_{\text{in, appl}}$ (ions nm^{-2})	$d_{\text{in, req}}$ (ions nm^{-2})	$d_{\text{in, appl}}$ (ions nm^{-2})	$d_{\text{in, req}}$ (ions nm^{-2})	$d_{\text{in, appl}}$ (ions nm^{-2})	$d_{\text{in, req}}$ (ions nm^{-2})
6.4	1×10^{17}	226	No blisters	251	No blisters	392	449 ± 17
	1×10^{18}	2260	No blisters	2510	501 ± 61	3923	469 ± 32
	1×10^{19}	22 600	No blisters	21 645	483 ± 47	39 231	512 ± 28
8.2	1×10^{17}	186	No blisters	216	No blisters	362	No blisters
	1×10^{18}	1862	No blisters	2156	661 ± 48	3625	679 ± 39
	1×10^{19}	18 622	No blisters	18 597	—	36 250	711 ± 37
10.1	1×10^{17}	159	No blisters	185	No blisters	323	No blisters
	1×10^{18}	1590	No blisters	1851	No blisters	3229	735 ± 42
	1×10^{19}	15 900	No blisters	15 966	—	32 286	757 ± 37
14.0	1×10^{17}	123	No blisters	143	No blisters	254	No blisters
	1×10^{18}	1230	No blisters	1432	No blisters	2537	No blisters
	1×10^{19}	12 304	No blisters	12 351	—	25 371	756 ± 30

but, after a typical time τ, the out-flux balances the in-flux, resulting in a time-independent profile. The time required to reach steady state, $\tau = t_f^2/D_{H_2,\text{eff}} = 4.11$ ms, is small compared to the total exposure time of $t > 40$ s and only the steady state fraction of hydrogen is considered in calculating the dose of hydrogen ions entering the blister volume.

The final hydrogen peak concentration is proportional to $\phi/D_{H_2,\text{eff}}$ and depends on the ion depth distribution from the SRIM calculation. As mentioned earlier, the maximum capacity to store hydrogen in the a-Si matrix, is about 10 atoms nm^{-3}. Given the measured in-flux of hydrogen, and assuming the SRIM profiles as the hydrogen source, the effective diffusion constant has to be at least $>1 \times 10^{-18}$ m^2 s^{-1}, as a smaller diffusion constant will lead to unacceptable high hydrogen concentrations in the blister cap.

In figure 9(b), the hydrogen fluxes as a function of time are shown. The double dotted dashed line shows the amount of hydrogen ions that are directly backscattered, as given by the SRIM calculation. The dashed line shows the out-diffusion of atomic hydrogen at the surface, and the solid line gives the atomic hydrogen flux into the blister volume. Figure 9(b) shows that most hydrogen is lost through the surface, and only a fraction $\phi_{\text{in}}/\phi \approx 0.19$ contributes to blister growth. At steady state, the total hydrogen out-flux is equal to the in-flux (29 ions nm^{-2} s, for 50 eV case shown in figure 9). Under steady state conditions, the fraction of the incoming flux that reaches the depth of delamination is only dependent on the initial hydrogen ion depth profile. This fraction is independent of the incoming flux and the diffusion constant.

Multiplying the measured applied hydrogen ion dose at the surface with the fraction that reaches the blister volume, as calculated by the one dimensional diffusion model, gives the local hydrogen in-flux to the blister volume, $d_{\text{in, appl}}$, as given in table 3. The local hydrogen dose decreases with increasing layer thickness and lower ion energies. In the cases for which blisters are observed, the calculated effective dose can be compared with the required ion dose $d_{\text{in, req}}$ (see figure 7). The uncertainty in $d_{\text{in, req}}$ is carried through from the standard deviation in the observed spread in blister radii.

At low incoming dose (10^{17} ions cm^{-2}) blisters are only observed for highest ion energy (100 eV) and thinnest multilayer (6.4 nm period). The calculated ion dose based on SRIM and the 1D diffusion model for this case ($d_{\text{in, appl}} = 392$ ions nm^{-2}) corresponds well to the required ion dose according to the pressurized blister model ($d_{\text{in, req}} = 449 \pm 17$ ions nm^{-2}).

For all other cases where blisters were observed, the calculated ion dose based on SRIM and the 1D diffusion model was significantly larger than the required ion dose according to the pressurized blister model (up to 77×). Studies on the hydrogenation of a-Si have shown that the hydrogen permeability of a-Si can change significantly during the hydrogenation process [54]. It is also known that increasing hydrogen concentration in the a-Si matrix, lowers the density of the a-Si and promotes the diffusivity of hydrogen [52].

The fact that diffusion increases with increased hydrogen concentration might also explain why no blisters were observed at incoming ion energies of 20 eV whereas the SRIM and 1D diffusion model with constant diffusion coefficient predict a dose which exceeds the ion dose required to form a blister. Figure 8 shows that in case of low energy ions (20 eV), the peak of the hydrogen distribution is close to the surface which likely leads to a larger diffusion coefficient towards the surface than into the multilayer.

A more accurate but complex description of the hydrogen penetration would include a diffusion constant that is dependent on the hydrogen concentration. The requirement for a dynamic diffusion constant is also supported by earlier research on blister formation in Mo/Si multilayers [27] and in c-Si substrates [55].

5. Conclusions

It has been observed in multiple cross sectional HRTEM images that delamination always occurred near the Mo-on-Si interface layer, which coincides with the position where *in situ* stress measurement show a strong (+4 N m^{-1}) tensile stress change. The stressed interface layer, therefore, acts as a preferential location for the initial delamination in the blister formation process.

Modeling indicates that a buckling instability of a compressively stressed layer does not play a dominant role in the blister formation. However a buckling instability, in combination with plastic deformation, might explain why the pressurized blister model underestimates the blister size by up to 20% for the larger multilayer thickness. Based on a pressurized blister model, the calculated pressure in the blisters ranges from 103–653 MPa.

Using a 1D diffusion model and SRIM calculations, the local ion dose at the location of blister formation was calculated for a wide range of ion energies (20 eV, 50 eV, 100 eV), incident fluxes (10^{17}, 10^{18}, 10^{19} ions cm^{-2}) and multilayer thicknesses (6.4 nm, 8.2 nm, 10.1 nm and 14 nm). In all cases a blister was observed, the calculated local ion dose was equal to or larger than the minimum local ion dose required according to the pressurized blister model (several hundred ions nm^{-2}). Comparing the required ion dose with the calculated applied ion dose, we found that, for ion energies $\geqslant$50 eV and multilayer periods of 6.4 and 8.2 nm, both ion doses are in agreement with the onset of blister formation. For multilayer periods of 10.1 and 14.0 nm the required dose, as calculated by a 1D diffusion model, overestimates the required ion dose. Above conclusions show that diffusion plays an essential element in blister formation.

Acknowledgments

The authors would like to thank Theo van Oijen for the multilayer sample preparation. This work is part of the research programme CP3E (Controlling photon and plasma induced processes at EUV optical surfaces) of FOM (Stichting voor Fundamenteel Onderzoek der Materie) with the financial support of NWO (Nederlandse organisatie voor Wetenschappelijk Onderzoek). The CP3E programme is co-financed by Carl Zeiss SMT and ASML.

ORCID iDs

R A J M van den Bos https://orcid.org/0000-0001-9446-2027

References

[1] Condon J B and Schober T 1993 *J. Nucl. Mater.* **207** 1
[2] Terreault B 2007 *Phys. Status Solidi* a **204** 2129
[3] Louthan M R 2008 *J. Fail. Anal. Prevention* **8** 289–307
[4] Koyama M, Akiyama E, Lee Y K, Raabe D and Tsuzaki K 2017 *Int. J. Hydrog. Energy* **42** 12706
[5] Robertson I M, Sofronis P, Nagao A, Martin M L, Wang S, Gross D W and Nygren K E 2015 *Metall. Mater. Trans.* A **46** 2323
[6] Bardamid A F *et al* 2006 *Plasma Devices Oper.* **14** 159
[7] Alimov V K, Roth J and Lindig S 2008 *J. Nucl. Mater.* **381** 267
[8] Xu H Y, Zhang Y B, Yuan Y, Fu B Q, Godfrey A, Temmerman G D, Liu W and Huang X 2013 *J. Nucl. Mater.* **443** 452
[9] ’t Hoen M H J, Dellasega D, Pezzoli A, Passoni M, Kleyn A W and Zeijlmans van Emmichoven P A 2015 *J. Nucl. Mater.* **463** 989
[10] Feng X Q and Huang Y 2004 *Int. J. Solids Struct.* **41** 4299
[11] Singh R, Christiansen S H, Moutanabbir O and Gösele U 2010 *J. Electron. Mater.* **39** 2177
[12] Lu G H, Zhou H B and Becquart C S 2014 *Nucl. Fusion* **54** 086001
[13] Griesche A, Dabah E, Kannengiesser T, Kardjilov N, Hilger A and Manke I 2014 *Acta Mater.* **78** 14
[14] Fukai Y 2005 *The Metal-Hydrogen System* 2nd edn (Berlin: Springer)
[15] Giguère A, Desrosiers N and Terreault B 2005 *Appl. Phys. Lett.* **87** 211911
[16] Eren B, Marot L, Günzburger G, Renault P O, Glatzel T, Steiner R and Meyer E 2014 *J. Phys. D: Appl. Phys.* **47** 025302
[17] Motai K, Oizumi H, Miyagaki S, Nishiyama I, Izumi A, Ueno T and Namiki A 2008 *Thin Solid Films* **516** 839
[18] Pelizzo M G, Corso A, Zuppella P, Windt D L, Mattei G and Nicolosi P 2011 *Opt. Express* **19** 14838
[19] Dolgov A, Lopaev D, Rachimova T, Kovalev A, Vasil’eva A, Lee C J, Krivtsun V M, Yakushev O and Bijkerk F 2014 *J. Phys. D: Appl. Phys.* **47** 065205
[20] Hutchinson J and Suo Z 1991 Mixed mode cracking in layered materials *Advances in Applied Mechanics* vol 29, ed J W Hutchinson and T Y Wu (New York: Academic) pp 63–191
[21] Hutchinson J W, Thouless M D and Liniger E G 1992 *Acta Metall. Mater.* **40** 295
[22] Goudeau P, George M and Coupeau C 2004 *Appl. Phys. Lett.* **84** 894
[23] Coupeau C, Dion E, David M L, Colin J and Grilhé J 2010 *Europhys. Lett.* **92** 16001
[24] Parry G, Coupeau C, Dion E, David M L, Colin J and Grilhé J 2011 *J. Appl. Phys.* **110** 114903
[25] Hong W J and Cheong S 2006 *J. Appl. Phys.* **100** 094322
[26] Mitani K and Gösele U M 1992 *Appl. Phys.* A **552** 543
[27] van den Bos R A J M, Reshetniak V, Lee C J, Benschop J and Bijkerk F 2016 *J. Appl. Phys.* **120** 235304
[28] Shao L *et al* 2005 *Appl. Phys. Lett.* **87** 091902
[29] Okba F, Cherkashin N, Di Z, Nastasi M, Rossi F, Merabet M and Claverie A 2010 *Appl. Phys. Lett.* **97** 031917
[30] Kuznetsov A S, Gleeson M A and Bijkerk F 2014 *J. Appl. Phys.* **115** 173510
[31] Kuznetsov A S, Gleeson M A and Bijkerk F 2013 *J. Appl. Phys.* **114** 113507
[32] van den Bos R A J M, Lee C J, Benschop J and Bijkerk F 2017 *J. Phys. D: Appl. Phys.* **50** 265302
[33] Timoshenko S and Woinowsky-Krieger S 1959 *Theory of plates and shells* 2nd edn (New York: McGraw-Hill)
[34] Zoethout E, Louis E and Bijkerk F 2016 *J. Appl. Phys.* **120** 115303
[35] Zubarev E N, Kondratenko V V, Pershyn Y P and Sevryukova V A 2011 *Thin Solid Films* **520** 314
[36] Vernon S P, Stearns D G and Rosen R S 1993 *Appl. Opt.* **32** 6969
[37] Yakshin A E, Louis E, Görts P, Maas E L G and Bijkerk F 2000 *Physica* B **283** 143

[38] Jergel M, Holý V, Majkovlá E, Luby Š, Senderák R R, Stock H J, Menke D, Kleineberg U and Heinzmann U 1998 *Physica* B **253** 28
[39] Bogdanova M A, Lopaev D V, Zyryanov S M and Rakhimov A T 2016 *Physics of Plasmas* **23** 073510
[40] Stoney G 1909 *Proc. R. Soc.* A **82** 172
[41] Janssen G C A M, Abdalla M M, van Keulen F, Pujada B R and van Venrooy B 2009 *Thin Solid Films* **517** 1858
[42] Feng X, Huang Y and Rosakis A 2007 *J. Appl. Mech.* **74** 1276
[43] Freitag J M and Clemens B M 1998 *Appl. Phys. Lett.* **73** 43
[44] Fokkema V 2011 *PhD Thesis* Leiden University
[45] Yokota K, Kageyama T and Katayama S 1985 *Solid-State Electron.* **28** 893
[46] Szekeres A and Danesh P 1996 *Semicond. Sci. Technol.* **11** 1225
[47] Freund L B and Suresh S 2003 *Thin Film Materials Stress* (Cambridge: Cambridge University Press)
[48] Kuschnereit R, Fath H, Kolomenskii A A and Szabadi M 1995 *Appl. Phys.* A **61** 269
[49] Evans A G and Hutchinson J W 1984 *Int. J. Solids Struct.* **20** 455
[50] SRIM www.srim.org/ (Accessed: July 2017)
[51] Ziegler J F, Biersack J P and Littmark U 1985 *The Stopping and Range of Ions in Matter* (New York: Pergamon)
[52] Schlatmann R, Keppel A, Xue Y and Verhoeven J 1993 *Appl. Phys. Lett.* **63** 3297
[53] Sharma B L 2005 *CRC Handbook of Chemistry and Physics* ed D R Lide (Boca Raton, FL: CRC Press) ch 12
[54] Beyer W 2016 *Phys. Status Solidi* a **213** 16611674
[55] Coupeau C, Parry G, Colin J, David M L, Labanowski J and Grilhé J 2013 *Appl. Phys. Lett.* **103** 031908